

Star Formation at Redshift One: H α from Multi-object Near Infrared Spectroscopy

M. Doherty¹, A.J. Bunker², R.G. Sharp³, I.R. Parry¹,
G.B. Dalton⁴, I. Lewis⁴, E. MacDonald⁴, C. Wolf⁴

¹Institute of Astronomy, University of Cambridge, UK (email: md@ast.cam.ac.uk)

²University of Exeter, UK ³Anglo-Australian Observatory, Australia ⁴Oxford Astrophysics, UK

We present preliminary results from a programme to obtain multi-object near-infrared spectroscopy of high redshift galaxies. Our project is to address the true star formation history of the universe at $z \sim 1$, a crucial epoch which some have suggested is the peak of star formation activity. By using H α -the same robust star formation indicator used at low- z - redshifted into the J- and H-bands, we can trace star formation without the systematic uncertainties of different calibrators, or the extreme dust extinction in the rest-UV, which have plagued previous efforts. We are using the instrument CIRPASS (the Cambridge Infra-Red Panoramic Survey Spectrograph; Parry et al. (2000)), which has been successfully demonstrated on the Anglo-Australia Telescope (AAT) and the William Herschel Telescope (WHT). CIRPASS has 150 fibres deployable over $\sim 40'$ on the AAT and $\sim 15'$ on the WHT, offering a huge multiplex advantage over traditional long slit spectroscopy.



Figure 2: Fibre plug-plate used to interface CIRPASS with the telescope.

We have used CIRPASS to measure star formation rates of a sample of galaxies at $z \sim 1$ in the Hubble Deep Field North (HDFN). This is the initial stage of a larger survey to address the true star formation history of the universe at redshifts $z=0.7-1.5$, through H α measurements. The wavelength coverage of CIRPASS is 1726Å, covering most of the J-band. It was set to a central wavelength of $\lambda_c \sim 1.25 \mu\text{m}$. With a resolving power of $R \sim 5000$, the background is very dark between the night sky OH lines in the J- and H-bands, with only about 10% of the array contaminated by skylines. By targeting galaxies with redshifts which place H α emission lines between the OH lines we become very sensitive to line emission, indeed we are limited by the instrument background rather than the sky. In an average fibre, between skylines, for a spectrally unresolved line we achieve a sensitivity of $1.0 \times 10^{-16} \text{erg s}^{-1} \text{cm}^{-2}$ at 5σ in 3 hours. However, the emission lines detected are typically broader than this ($100 - 150 \text{ km s}^{-1}$).

id	RA (J2000)	Dec (J2000)	$\lambda_{\text{H}\alpha}$ (Å)	z_{opt}	$z_{\text{H}\alpha}$	fwhm (Å)	Vel. fwhm km s^{-1}	flux $\times 10^{-16}$ $\text{erg cm}^{-2} \text{s}^{-1}$
J1236175+6214027	12 36 17.526	+62 14 02.70	11921	0.818	0.816	6.6	146	3.57
J1237063+6215185	12 37 06.293	+62 15 18.50	12078	0.84	0.840	6.9	153	5.69
J1237084+6215150	12 37 08.381	+62 15 15.04	12074	0.839	0.840	6.9	153	2.26
J1237087+6211285	12 37 08.659	+62 11 28.52	12520	0.907	0.908	7.2	161	4.71
J1237141+6210448	12 37 14.141	+62 10 44.78	11952	0.821	0.821	5.8	124	4.24
J1237166+6210424	12 37 16.631	+62 10 42.36	11950	0.821	0.821	5.4	114	1.90
J1237167+6213105	12 37 16.716	+62 13 10.54	12465	0.898	0.898	4.8	97	2.96

Table 1: Measured properties of the H α emission lines in our $>5\sigma$ detections in the HDF-N. The optical redshifts are from Cohen et al. (2000)

Acknowledgements

CIRPASS was built by the IoA, Cambridge, with the generous support of the Raymond and Beverly Sackler Foundation and PPARC. We thank the staff at the WHT for their help in enabling CIRPASS to be used as a visitor instrument.

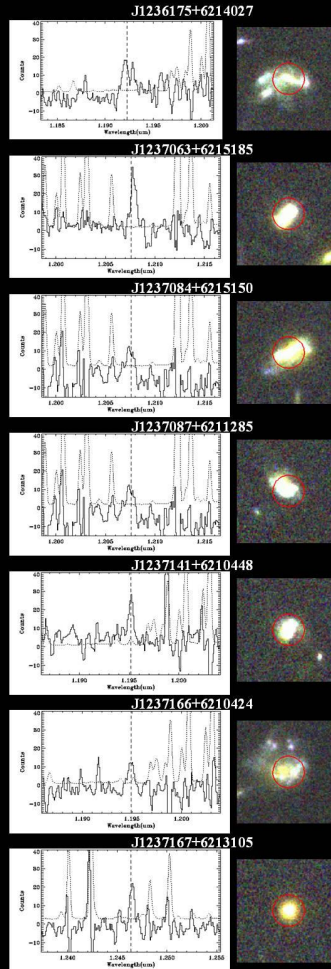


Figure 1: Spectra and three colour images for the seven brightest H α detections in our sample. The expected position of H α at the optical spectroscopic redshift is marked with a dashed line. The sky spectrum is overlaid with dotted lines. The three colour images are made from GOODS B, i, z' images and the fibre size ($1.1''$) is shown by a red circle.

We present here observations of seven sources where H α was detected with a signal to noise of more than 5σ . The emission line spectra are shown in Figure 1. We accurately measured integrated line fluxes using two methods:

- by measuring between the zero power points and
- by fitting gaussian profiles to the lines,

which also gave the full width at half maximum (FWHM) for each. Key measurements for each H α emission line are shown in Table 1, which gives the central wavelength and corresponding redshift of the line, its full width at half maximum in wavelength and velocity and total line flux.

The H α luminosity of a galaxy is proportional to the number of OB stars, therefore in order to extrapolate to a total SFR it is necessary to assume a certain initial mass function (IMF). We use the conversion given in Kennicutt (1998):

$$\text{SFR}(M_{\odot} \text{yr}^{-1}) = 7.9 \times 10^{-42} I_{\text{H}\alpha} (\text{erg s}^{-1})$$

The derived SFRs of the galaxies are shown in Table 2, and in Figure 1 we show B, V, i', and z' band images from HST/ACS taken from GOODS v1.0 (Giavalisco et al. 2003). We performed photometry on these images with $1''$ apertures, for consistency with our infrared fibre size, and used the B band magnitudes (4500Å) to calculate rest frame UV (2400Å) flux densities and corresponding star formation rates, which are also shown in Table 2. For consistency, we also use the conversion given in Kennicutt (1998), which assumes the same IMF as the SFRs derived from the H α flux. In most cases the $1.1''$ fibres enclose most of the B band light, however, for three of the sources, some fraction ($\sim 20\%$) is missed. SFRs for these objects calculated from UV luminosities, compared to those calculated from the H α flux, are underestimated by a factor 2-3, probably due to extinction by dust. This is consistent with results obtained by Glazebrook et al. (1999), Tresse et al. (2002) and Yan et al. (1999).

id	SFR $_{\text{H}\alpha}$ $M_{\odot} \text{yr}^{-1}$	B $_{AB}$ mag	Flux density L_{ν} $10^{28} \text{erg s}^{-1} \text{Hz}^{-1}$	SFR $_{\text{UV}}$ $M_{\odot} \text{yr}^{-1}$
J1236175+6214027	10	23.89	1.07	2.5
J1237063+6215185	17	22.89	2.84	6.6
J1237084+6215150	7	23.33	1.70	3.9
J1237087+6211285	17	23.23	2.37	5.6
J1237141+6210448	12	23.32	1.83	4.2
J1237166+6210424	5	23.85	1.13	2.6
J1237167+6213105	11	23.96	1.19	2.8

Table 2: Identification, SFR derived from H α , B magnitude and corresponding flux density and SFR $_{\text{UV}}$ for our $>5\sigma$ detections.



Figure 3: Positioning the fibres on the brass plug plate

References

- Cohen et al. 2000, ApJ, 538, 29
Giavalisco et al. 2003, AAS 202
Glazebrook et al. 1999, MNRAS, 306, 843
Kennicutt 1998, ARA&A, 36, 189
Parry et al. 2000, SPIE 4008, 1193
Tresse et al. 2002, MNRAS, 337, 369
Yan et al. 1999, ApJ, 519, L47